

# Intrinsic point defects and volume swelling in $\text{ZrSiO}_4$ under irradiation

J.M. Pruneda,\* T. D. Archer,† and Emilio Artacho

*Department of Earth Sciences, University of Cambridge Downing Street, Cambridge, CB2 3EQ, United Kingdom*

(Dated: November 12, 2018)

The effects of high concentration of point defects in crystalline  $\text{ZrSiO}_4$  as originated by exposure to radiation, have been simulated using first principles density functional calculations. Structural relaxation and vibrational studies were performed for a catalogue of intrinsic point defects, with different charge states and concentrations. The experimental evidence of a large anisotropic volume swelling in natural and artificially irradiated samples is used to select the subset of defects that give similar lattice swelling for the concentrations studied, namely interstitials of O and Si, and the anti-site  $\text{Zr}_{\text{Si}}$ . Calculated vibrational spectra for the interstitials show additional evidence for the presence of high concentrations of some of these defects in irradiated zircon.

PACS numbers: 61.72.-y, 61.80.-x, 78.30.-j

## I. INTRODUCTION

Large concentration of defects in materials produce strains that affect the crystalline lattice structure, which can undergo amorphization, change into a different crystalline phase, or remain in the same crystal phase with changes in the lattice parameters. In addition to these changes, the electronic properties are affected in a way that can produce substantial differences in the physical and chemical properties of the original material. Radiation effects in ceramic materials have been subject of a considerable number of studies due to their use in nuclear fusion applications, and in the stabilization and immobilization of nuclear high-level waste<sup>1,2</sup>. Defect accumulation and its consequences for the degradation of the mechanical properties have to be understood in order to control possible leaching, creep and fatigue of these materials. A number of issues have to be investigated, such as the stabilities of possible defects, their structure, migration energies for interstitials and vacancies, displacement threshold energies, defect interactions and clustering, and their electronic structure.

Zircon ( $\text{ZrSiO}_4$ ) has attracted considerable attention due to several physical properties of interest, such as high permittivity (zirconium silicates are candidates as a gate dielectric in future silicon field effect transistors<sup>3</sup>), low thermal conductivity and high chemical stability. It has also been proposed as a ceramic host for the immobilization of nuclear waste due to its high ability to accommodate actinides by substitution of Zr, and its high resistance to corrosion<sup>1,4</sup>. Natural zircon may contain uranium in concentrations of up to 20,000 ppm, and samples with up to 4 billion years have been dated. Thus, even if possibly not the best final material for nuclear waste encapsulation, it is an ideal system to study the effects of radiation damage.

After a radioactive impurity undergoes an  $\alpha$ -decay transition, strong damage is produced in the crystalline structure. The heavy recoiling atom (tens to hundreds of keV) propagates through the material losing energy mainly through atomic collisions, thus producing large cascade collisions and in consequence, amorphized re-

gions. The highly energetic  $\alpha$  particle ( $\sim 5$  MeV) that propagates in the opposite direction to the recoil atom, dissipates most of its energy by ionization processes, and a relatively smaller number of atomic displacements mainly at the end of its path.

When the dose of  $\alpha$ -decays is not too large there is a coexistence between the amorphized (metamict) region and the crystalline phase, the latter containing point defects. Barriers to recombination cause the accumulation of large concentration of these defects, resulting in changes of the unit cell volume and shape. This swelling is measured from the shifts in the reflection angle in X-ray diffraction (XRD) and it is clearly distinct from the one produced by the amorphous region, observed by changes in the total density.

Experiments based on natural samples, Pu-doped zircon and ion-beam irradiation, show a unit cell volume expansion of up to 5%. This volume swelling is anisotropic, giving an increase of  $\sim 1.5\%$  along the  $ab$ -axis, and  $\sim 2\%$  along the  $c$ -axis<sup>5</sup>. Over geological periods the recovery of a large fraction of point defects is observed in natural zircons (as opposed to Pu-doped samples<sup>5,6</sup>), with preferential self-annealing of the  $ab$  plane<sup>7</sup>.

Characterization of structural changes in the crystalline phase<sup>7</sup> show that the dodecahedron  $\text{ZrO}_8$  is the less stable unit in zircon, and the defects are expected to be more closely related to it, as the Si atoms are well confined in the  $\text{SiO}_4$  tetrahedra. Theoretical studies of neutral point defects show that the oxygen interstitial is the most stable one<sup>8</sup>. A non negligible concentration is expected at thermal equilibrium. The energies required to form native defects in zircon were investigated by molecular dynamics simulations of primary-knock-on-atom collisions with empirical potentials<sup>9</sup>. It was shown that the effective energy required to displace O from its crystal position is  $\sim 17$  eV, whereas it is larger for Si and Zr ( $\sim 48$ , and  $\sim 60$  respectively).

The previous theoretical studies of point defects in zircon were focused on the energetics of neutral defects. However, due to ionization processes produced by the  $\alpha$ -particle, and the fact that the resulting defect landscape affects the electronic chemical potential, the de-

fects can be charged. The accumulation of charged defects produce electric fields that would change the kinetics of accumulation and diffusivity. In the present work, we use first principles electronic structure calculations to study the influence of very high concentration of neutral and charged point defects on the crystalline structure of  $\text{ZrSiO}_4$ . We perform structural relaxations, studying electronic properties, as well as some spectroscopic calculations of a wide variety of defects, forming a quite complete catalogue that is compared with experimental data. The effects of order/disorder of these defects have not been considered in the present study, where periodic supercells were used to describe them.

## II. METHODOLOGY

Calculations of the electronic properties of  $\text{ZrSiO}_4$  are performed with the self-consistent *ab initio* SIESTA method<sup>10</sup>, using Density Functional Theory (DFT)<sup>11</sup> within the Local Density Approximation (LDA)<sup>12</sup>. The core electrons are replaced by norm-conserving pseudopotentials<sup>13</sup> in the Kleinman-Bylander form<sup>14</sup>, generated with  $\text{Zr}(4s^2, 4p^6, 4d^2, 5s^2)$ ,  $\text{Si}(3s^2, 3p^2)$ , and  $\text{O}(2s^2, 2p^4)$  atomic valence configurations. The 4p electrons in Zr were explicitly included in the calculations as semicore states, due to the large overlap with the valence states. The wave functions are described with linear combinations of strictly localized numerical atomic orbitals<sup>15</sup>. We used a single- $\zeta$  basis set for the semicore states of Zr, and double- $\zeta$  plus polarization for the valence states<sup>16</sup>. The charge density is projected on a real space uniform grid with an equivalent plane-wave cut-off of 227 Ry, to calculate the exchange-correlation and Hartree matrix elements.

To simulate the defect structures, the host crystal is represented by a supercell generated by repetition of the conventional tetragonal unit cell (4 formula units). The point defect is then introduced inside this supercell (adding atoms for interstitial, removing atoms for vacancies, etc), that have to be of the right size to describe the sought large defect concentrations. We use host supercells with 24, 48, and 96 atoms. The supercell with 48 atoms is a repetition of the tetragonal cell along the  $c$  axis, and the one with 96, is a repetition along the  $a$  and  $b$  axis. In this way, different concentrations of defects can be simulated by changing the number of repetitions in the cell. The supercells with 24 and 48 atoms were already used by Crocombette in his study of points defects, and he estimated that unreal physical interaction between periodic images of the defects was of the order of 0.5 eV. For the high concentrations we are interested in, these interactions between defects are expected and only their periodic arrangement might be unrealistic. The use of more than one defect per supercell can alleviate this approximation, and will be discussed later.

Simulating charged defects with periodic boundary conditions, requires handling with care the long-range

coulombic interactions. The unphysical divergence in the energy coming from the long range Coulomb interactions of a periodic array of charges is compensated by a uniform electron-charge neutralizing background<sup>17</sup>. The minimum-energy structure for each defect was obtained by relaxing with a conjugate-gradient minimization for the forces and stresses. The lattice vectors and the atomic positions were allowed to relax until atomic forces and stresses from the electronic structure calculations were smaller than  $30 \text{ meV}/\text{\AA}$  and  $6 \text{ meV}/\text{\AA}^3$ , respectively. The formation energies of the defects in the different charge states are function both of the electron chemical potential  $\mu_e$ , and of the atomic chemical potentials for the species involved in the defect, and will be discussed elsewhere<sup>18</sup>.

The local vibrational modes (LVM) associated to the defects are obtained from the dynamical matrix in the relaxed structure, by finite differences, i.e. computing the energies with each atom displaced by  $\sim \pm 0.016 \text{\AA}$  along each of the cartesian coordinates. The eigenvalues and eigenvectors of the dynamical matrix give the vibrational frequencies and eigenmodes in the harmonic approximation. Previous studies show a deviation of  $\sim 5\%$  for vibrational frequencies of point defects in semiconductors.

The Born-effective charge tensors,  $Z_{ij,\alpha}^*$ , are used to determine the infrared intensities, and the splitting between longitudinal (LO) and transverse (TO) optic modes<sup>20</sup>. They are computed by finite differences as the change in the  $i$  component of the polarization (computed with the Berry phase formalism<sup>21</sup>) when the atom  $\alpha$  is displaced along the  $j$  direction.

## III. CRYSTAL $\text{ZrSiO}_4$

Zircon ( $\text{ZrSiO}_4$ ) has tetragonal  $I4_1/amd$  space group. The structure consists of alternating  $\text{SiO}_4$  tetrahedra and  $\text{ZrO}_8$  triangular dodecahedra sharing edges and forming chains parallel to the crystallographic  $c$  axis (Fig. 1). A body-centred unit cell can be chosen, containing four formula units. The structure is fully described with 4 parameters (see table I): The lattice constants  $a$  and  $c$ , and the internal parameters  $y$  and  $z$ . Zirconium and silicon atoms are located in the  $4a$  and  $4b$  Wyckoff positions,  $(0, \frac{3}{4}, \frac{1}{8})$  and  $(0, \frac{1}{4}, \frac{3}{8})$ , respectively, and the oxygen atoms in the  $16h$  sites  $(0, y, z)$ . Each O is shared between one Si and two Zr atoms, at distances 1.62, 2.12 and  $2.25 \text{\AA}$  respectively. These 4 atoms are in the O-site's mirror plane that can be perpendicular to the  $a$  or  $b$  axis. The relaxed parameters calculated are in good agreement with experimental values.

The Born effective-charge tensor is shown in table II and is in excellent agreement with the results obtained with linear response calculations<sup>22</sup>. Because of the local symmetry in the Zr and Si sites, the Born charge tensors for these atoms are diagonal, with only two independent components,  $Z_{\parallel}^*$  and  $Z_{\perp}^*$  parallel and perpendicular to the crystallographic  $c$ -axis, respectively. The large value

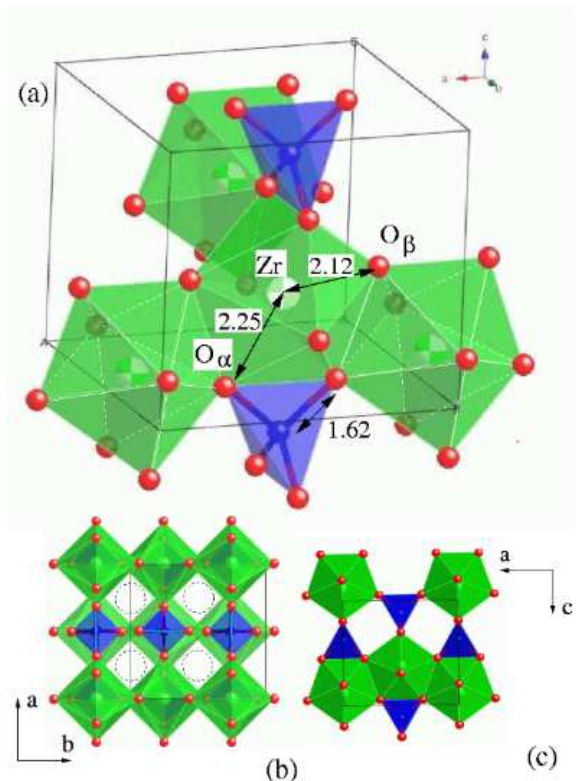


FIG. 1: (*Color Online*) (a) Edge-sharing Si-tetrahedra and Zr-dodecahedra along the  $c$ -axis, corner sharing in the  $ab$ -plane. The dodecahedra also have edge-sharing with each other along the  $ab$ -plane. (b) and (c) show the projection of the unit cell in the  $ab$  plane, and in a plane perpendicular to the  $b$  axis (the second layer of polyhedra has been removed in (c) for a better visualization). The dashed circles in (b) show the empty spaces in which we place the interstitials.

of  $Z_{Zr}^*$  and  $Z_{Si}^*$  with respect to the nominal ionic electronic charge is interpreted in terms of mixed covalent-ionic bonding due to hybridization with oxygen<sup>22</sup>. For O, the Born charge tensor is anisotropic, with the charge in the mirror plane being larger than the nominal ionic charge ( $Z=-2$ ), and the tensor component perpendicular

TABLE I: Calculated structural parameters for crystalline  $ZrSiO_4$  compared to experimental values.

	This work	Ref. [22]	Experiment <sup>23</sup>
Volume	129 ( $\text{\AA}^3$ )	127	131
a	6.59 ( $\text{\AA}$ )	6.54	6.61
c	5.96 ( $\text{\AA}$ )	5.92	5.98
y	0.068	0.0645	0.0661
z	0.184	0.1945	0.1953
$d(\text{Si-O})$	1.62	1.61	1.62
$d(\text{Zr-O}^\alpha)$	2.25	2.24	2.27
$d(\text{Zr-O}^\beta)$	2.12	2.10	2.13
$\widehat{O-Si-O}$	$96^\circ$	$97^\circ$	$97^\circ$
	$116^\circ$	$116^\circ$	$116^\circ$

to the mirror plane being smaller.

Seven infrared active modes ( $3A_{2u}+4E_u$ ) are predicted by group theory in  $ZrSiO_4$  at  $\Gamma$ . The induced polarization for  $E_u$  modes is perpendicular to the  $c$  axis, while  $A_{2u}$  modes are observed for electric field vectors parallel to  $c$ . The spectrum between  $650$  and  $1400 \text{ cm}^{-1}$  is characterized by Si-O stretching vibrations ( $E_u(4)$  and  $A_{2u}(3)$  modes respectively<sup>19</sup>) and the O-Si-O bending modes  $E_u(3)$  and  $A_{2u}(2)$ . Our computed frequencies for these modes are  $851, 969, 414,$  and  $602 \text{ cm}^{-1}$  respectively, with a maximum deviation of  $3.8\%$  with experiments. The modes below  $400 \text{ cm}^{-1}$  are related to  $\text{SiO}_4$  group motions against Zr atoms, and motions of Zr atoms.

## IV. POINT DEFECTS

We have considered a catalogue of neutral and charged intrinsic defects, that includes interstitials ( $X_i$ ) and vacancies ( $V_X$ ) of the three elements ( $X$ ) present in zircon, Zr and Si anti-site defects ( $Zr_{Si}$ , and  $Si_{Zr}$ ), Frenkel pairs ( $X_{FP}$ ), and other combinations of interstitials and vacancies.

### A. Volume swelling

The effect of point defects in the lattice structure after relaxation is summarized in Fig. 2, where we show the change in the lattice parameters relative to the neutral structure for the defects studied. Some defects produce a considerable distortion of the crystalline lattice, whereas others such as oxygen interstitial, or the vacancies have a much smaller effect. The magnitude of the distortion depends on the concentration of defects (supercell size in our study). For the values of interest in this work, a clear trend is observed, with an almost linear dependence between the distortion and the concentration (see Fig. 3). For the highest concentration studied (one defect per unit cell), we explored the effect of defect disorder by introducing two point defects in the supercell made from two unit cells. Fig. 3 shows a dispersion in the swelling due to the different configurations studied in this

TABLE II: Born effective charge tensors for Zr, Si, and O atoms. The Born charge for O, correspond to the atom located at  $(0, u, v)$ , with the mirror plane perpendicular to  $x$ . For Zr and Si, only the diagonal elements are shown. For O, the whole charge tensor is presented, as well as the corresponding eigenvalues. See also Ref. [22]

$Z_{Zr}^*$	(5.33 5.33 4.66)	
$Z_{Si}^*$	(3.21 3.21 4.38)	
$Z_O^*$	$\begin{pmatrix} -1.19 & 0 & 0 \\ 0 & -3.11 & -0.15 \\ 0 & -0.34 & -2.26 \end{pmatrix}$	$\begin{bmatrix} -1.19 \\ -3.16 \\ -2.20 \end{bmatrix}$

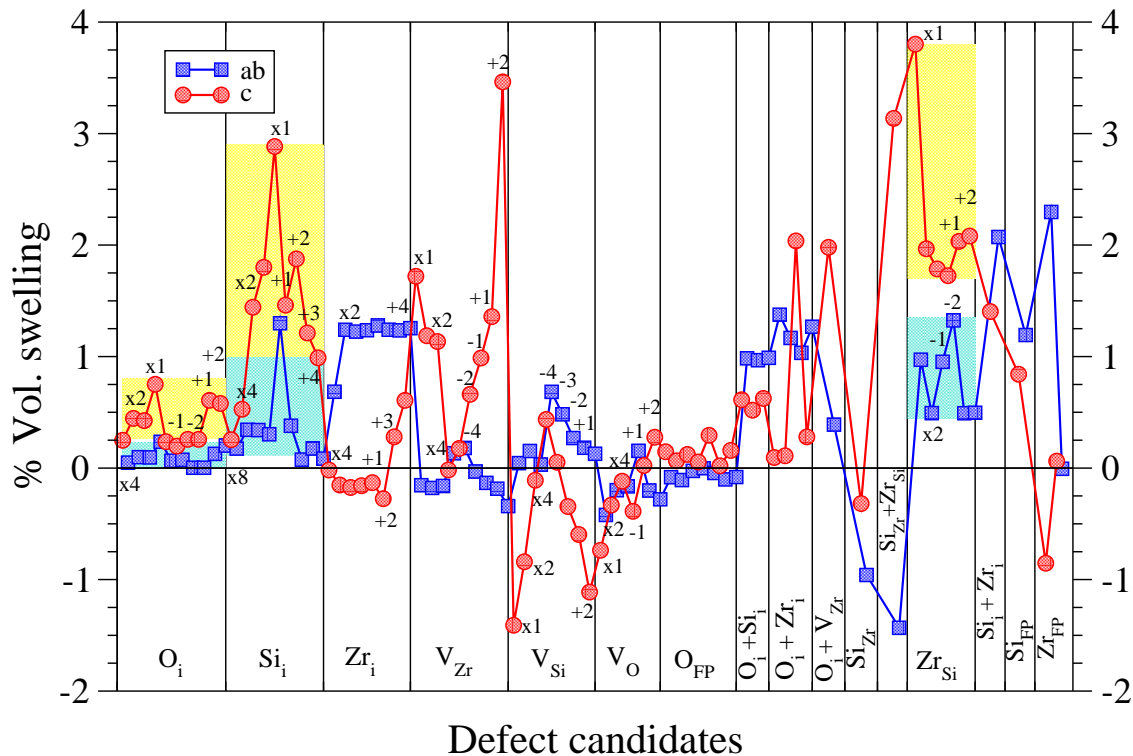


FIG. 2: (*Color online*) Lattice parameter swelling (in %) for the set of defects considered in this work. An average in the basal (*ab*) plane is done to compare with the relaxed crystalline structure.  $X_i$ ,  $V_X$ ,  $X_{FP}$  denote interstitials, vacancies and Frenkel pairs of  $X$ , respectively. The different charge states are denoted by  $\pm q$  and the different concentrations of defects by  $\times n$ , with  $n$  denoting the number of repetitions of the tetragonal unit cell (cells with 24, 48 and 96 atoms, for  $n = 1, 2, 4$  respectively). Unless stated, the neutral defect with  $n = 2$  cell is considered.

way. Even if the effect is sizeable it does not affect our arguments or conclusions, though further work in this direction will be needed.

In general, there is a considerable anisotropy in the relaxation, with different changes in the  $c$ -axis and in the  $ab$ -plane. Experimentally<sup>5</sup>, an increase in  $c$  of  $\sim 2\%$  is observed, while  $a$  increases by a smaller amount ( $\sim 1.5\%$ ). Based in this evidence, we can focus our study on those defects that give a behaviour in the lattice swelling similar to the one observed, eliminating those that produce a decrease in the cell parameters, or a larger change in  $a$

than in  $c$ . The defects with the stronger distortions are the interstitial of silicon,  $Si_i$ , and the anti-site of zirconium in the position of silicon,  $Zr_{Si_i}$ . The calculations for charged systems were done with the supercell of 2 tetragonal unit cells, repeated along the  $c$ -axis. The artificial coulomb interaction between cells should be then more important in the  $ab$ -plane, but we observed that the lattice parameter  $c$  is more strongly affected by the charge state than  $ab$ .

## B. Structural relaxation and electronic structure.

### 1. Interstitials

Initially, we place the interstitial atoms in regions with empty space (see dashed circles in Fig. 1), and perform conjugate gradient minimization of the forces and stresses. We have explored different starting points, showing here the relaxed structures with minimum energy.

For  $Zr_i$  and  $Si_i$  the interstitial remains along the  $c$ -axis empty spaces (Fig. 1b). Nevertheless, the lattice is strongly distorted and the  $SiO_4$  and  $ZrO_8$  polyhedra

TABLE III: Frequencies for IR active modes in  $ZrSiO_4$  (in  $cm^{-1}$ ).

Mode	This work	Ref. [22]	Expt. <sup>19</sup>
$A_{2u}(1)$	371	348	338
$A_{2u}(2)$	602	601	608
$A_{2u}(3)$	969	979	989
$E_u(1)$	295	285	287
$E_u(2)$	402	383	389
$E_u(3)$	414	422	430
$E_u(4)$	851	867	885

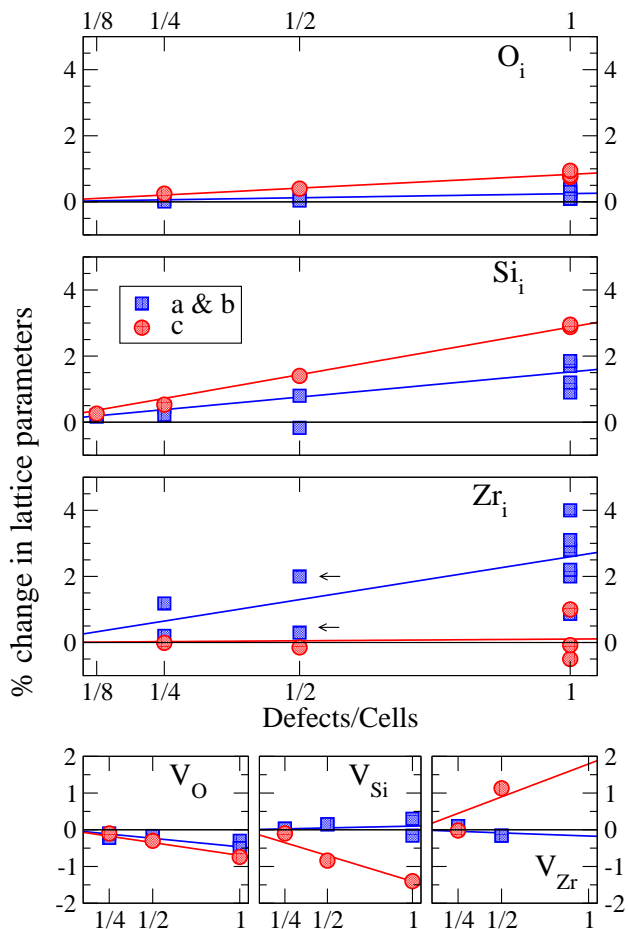


FIG. 3: (Color online) Change in lattice constants (%) as a function of the concentration of defects, for interstitials and vacancies of the three constituent elements. Results are shown for 1 defect for each  $N$ -repetitions of the tetragonal unit cell, with  $N = 1, 2, 4$  and  $8$ . The small arrows show the anisotropic swelling in the  $ab$  plane for  $Zr_i$ . The different points for 1 defect/cell refer to different disorder realizations.

change to accommodate to the presence of the interstitial. There is an anisotropic change in the lattice parameters. While  $Zr_i$  produces large orthorhombic distortion in the basal plane (with an increase of up to 3% in the  $a$  lattice parameter, for a concentration of 1 defect in two unit cells, and smaller distortions in the other parameters), the  $Si_i$  distorts the crystal mainly in the  $c$ -axis, but also in the other directions. Upon removal of electrons from  $Si_i$ , new atomic structures are obtained, with the interstitial causing oxygen atoms to approach, and neutralize the charge around it. In this way, the coordination of  $Si_i^{+n}$  increases with  $n$  and for  $Si_i^{+4}$  a six-fold coordinated structure results, with Si-O bonds slightly longer ( $\sim 1.8\text{\AA}$ ) than in the initial tetrahedral geometry. In Fig. 4 we show the electronic deformation density (difference between the solid and atomic electronic clouds),  $\delta\rho$ , around  $Si_i$  in two different planes. The geometries for positively charged Zr-interstitials are basically unchanged with re-

spect to the neutral structure.

In agreement with previous theoretical studies<sup>8</sup>, we observe that the neutral  $O_i$  forms a “dumbbell”-like structure (see Fig. 5a), with the axis almost perpendicular to the mirror plane of the oxygen in the crystal position. The distances between both oxygen atoms, and the neighbouring cations are shown in table IV. A similar structure was also observed in calculations of interstitial O in  $ZrO_2$ <sup>24</sup>. The high ionicity of the crystal forces the interstitial to a position where the electronic density screens the coulomb interactions. The covalent bond to the interstitial oxygen reduces the strength of the Si-O bond, and the  $SiO_4$  tetrahedra loses part of its charge. Mulliken population analysis shows that the charges in the interstitial and in the lattice oxygen are similar, and slightly smaller (6%) than in other oxygen atoms.

The structure of charged  $O_i^-$  does not differ substantially from the neutral defect, with a slight increase of the  $O_i^-$ -O distance (see table IV). On the contrary, the doubly charged interstitial displaces from the dumbbell structure, and forms a bridge between neighbour silicon atoms, both having now coordination five. In this structure, the relaxed  $O_i^{2-}$ - $O_A$  distance (2.19 Å) does not admit a bond between the oxygens, while  $Si_A$ - $O_i^{2-}$  and  $Si_B$ - $O_i^{2-}$  do (1.74 and 1.78 Å, respectively). This can be seen in Fig. 5d, where  $\delta\rho$  around the interstitial oxygen differs from the one in the neutral defect (Fig. 5c). The electronic cloud along the  $Si_A$ - $O_i$ - $Si_B$  directions (Fig. 5e) resembles the Si-O bond in the crystalline configuration. The relaxation energy from the initial dumbbell configuration is of about 1.6 eV, while the energy of the neutral defect in the atomic structure of  $O_i^{2-}$  is 2.9 eV higher.

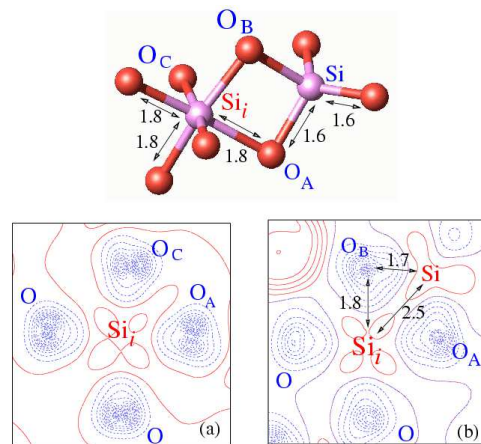


FIG. 4: (Color online) Atomic configurations for silicon interstitial in the +4 charged state and corresponding charge density-deformation contour plot in the plane defined by  $Si_i$ ,  $O_A$  and  $O_C$  (a), and  $Si_i$ ,  $O_A$  and  $O_B$  (b). Distances given in Å and the contour plots are drawn between  $-0.45$  and  $0.45e$ , with a step of  $0.015e$ . Solid (dashed) lines correspond to negative (positive) values for the charge.

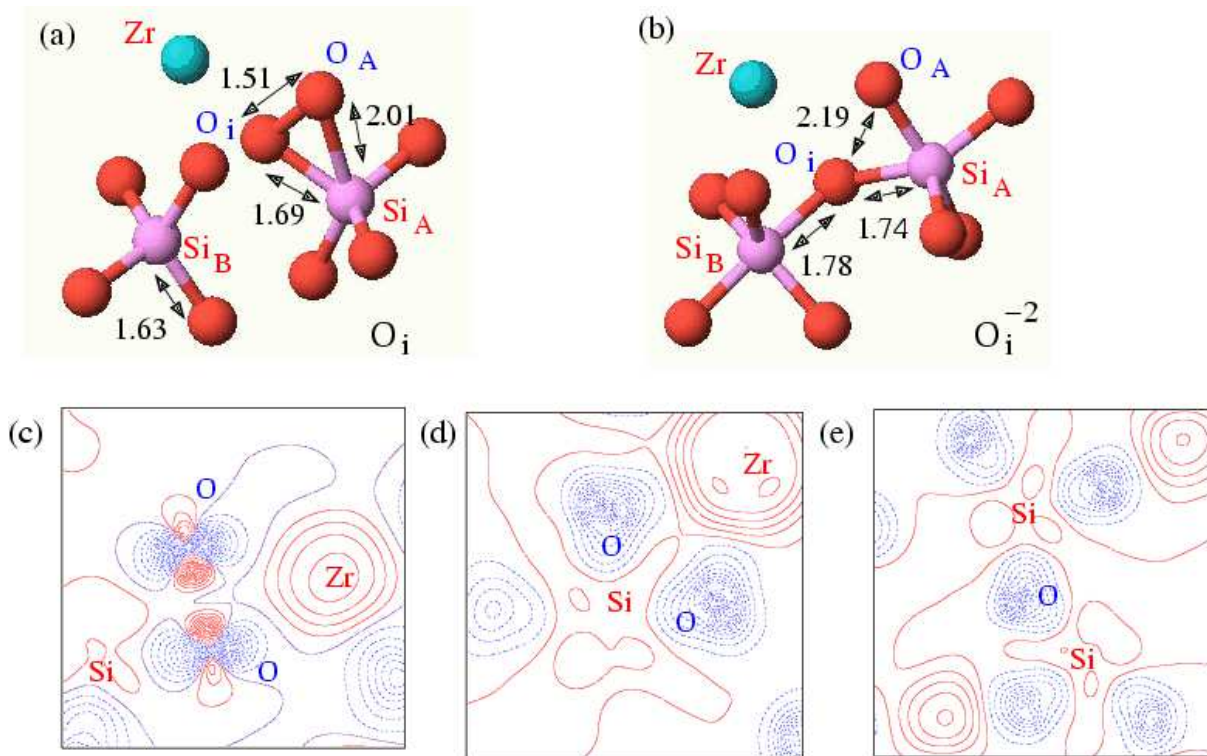


FIG. 5: (*Color online*) Atomic configurations for oxygen interstitials in the neutral (a) and doubly negatively charged (b) states, and corresponding deformation density contour plots in the plane defined by  $\text{Si}_A$ ,  $\text{O}_A$  and  $\text{O}_i$  (c and d for neutral and charged configurations, respectively). (e) shows the contour plot in the plane through  $\text{Si}_A$ ,  $\text{O}_i$  and  $\text{Si}_B$ , in  $\text{O}_i^{-2}$ . Distances given in Å and the contour plots are drawn between  $-0.45$  and  $0.45e$ , with a step of  $0.015e$ . Solid (dashed) lines correspond to negative (positive) values of the deformation density.

## 2. Vacancies

In the  $V_O$ , the silicon atom moves slightly in the direction of the missing oxygen, and the remaining Si-O bond lengths are increased by 4%. A new electronic state is created in the gap, localized around the vacancy. In the charged defect  $V_O^+$ , the Si atom moves back toward its initial position, and the Si-O bonds have deviations smaller than 1% with respect to the original Si-O tetrahedra.

TABLE IV: Interatomic distances in the dumbbell structure (in Å), for different concentration of defects (supercells with 24, 48 and 96 atoms). Charged defect is within the supercell containing 48 atoms.

	24	48	96	Ref.[8]	$\text{O}_i^-$
$\text{O}_i\text{-O}_A$	1.52	1.52	1.52	1.62	1.99
$\text{O}_i\text{-Si}$	1.96	1.69	1.70	1.83	1.69
$\text{O}_i\text{-Zr}_1$	2.29	2.24	2.23	2.24	2.15
$\text{O}_i\text{-Zr}_2$	2.22	2.84	2.82	2.57	2.98
$\text{O}_A\text{-Si}$	1.70	2.00	1.95	1.78	1.80
$\text{O}_A\text{-Zr}_1$	2.24	2.23	2.30	2.20	2.32
$\text{O}_A\text{-Zr}_2$	2.84	2.22	2.22	2.75	2.18

The four oxygen atoms forming the tetrahedra around the silicon vacancy remain in their position, with only minor deviations towards their centre of mass ( $\sim -0.7\%$ ). For the  $V_{\text{Si}}^{-n}$  configurations, the oxygen tetrahedron expands, with the distance from the centre of mass increasing by 2% for  $n = 1$  and by 5% for  $n = 2$ . For the  $V_{\text{Zr}}$  defect a similar effect is observed for the oxygen atoms forming the dodecahedra. There is a considerable expansion of the  $V_{\text{Zr}}\text{-O}^\alpha$  bond ( $\sim 10\%$ ), and a smaller change in the  $V_{\text{Zr}}\text{-O}^\beta$  length ( $\sim +4\%$ ), that explains the anisotropic change in lattice parameters. The expansion of the  $V_{\text{Zr}}\text{-O}^v$  bond increases for the negatively charged vacancies. The  $V_{\text{Zr}}\text{-O}^i$  length expansion decreases (increases) for negatively (positively) charged vacancies.

## 3. Frenkel pairs and anti-sites

Frenkel pairs of Zr and Si are not favourable because of the strong ionic interaction between the interstitial and the vacancy. There is a trend for the interstitial to move towards the open space of the vacancy, and a restitution was observed in the relaxation of several initial structures considered. In the case of  $\text{O}_{FP}$ , the interstitial and the vacancy do not interact strongly, and the final configu-

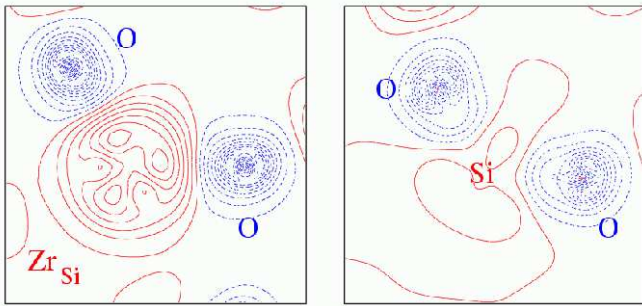


FIG. 6: (*Color online*) Charge redistribution density around  $Zr_{Si}$  and Si, in the tetrahedral plane.

ration is similar to an isolated vacancy and a dumbbell interstitial, even when both are in the same Si-O tetrahedra.

In the  $Si_{Zr}$  anti-site, the Si atom substitutes a Zr atom in the center of the dodecahedron, with a reduction of the lengths (-4% for Si-O<sup>i</sup> and -6% for Si-O<sup>v</sup>). In  $Zr_{Si}$ , the Zr forms a tetrahedron with four oxygen around it, with bond lengths of 1.9Å (+17% longer than the Si-O bonds). The Si-O distances increase slightly ( $\sim +1\%$ ) close to the defect, due to the increase in the lattice parameters. Fig. 6 shows the contour plot of  $\delta\rho$  in the plane defined by  $Zr_{Si}$  and a pair of oxygens in the tetrahedron. In the charged configurations, the bond lengths do not change substantially.

### C. Vibrational properties

The infrared (IR) reflection and absorption spectra of zircon is considerably affected by radiation damage. Changes in peak frequency, decrease in band intensity, and line broadening of the spectra of crystalline zircon can be related to changes in the lattice bond lengths. In addition, new features appear for highly damaged samples, with an increase in the IR intensity with increasing dose. One of the new spectral features is the appearance of an absorption sharp peak near  $796\text{ cm}^{-1}$  in moderately damaged zircon<sup>25</sup>. This peak is in a gap of the vibrational density of states (VDOS) of crystalline zircon. Its origin is unclear, and it has been proposed that it could be due to a radiation-induced intermediate phase, or to distortions in the boundaries between crystalline and amorphized regions<sup>25</sup>.

We computed the vibrational properties for interstitials of O, Si and Zr, and for the anti-site defect  $Zr_{Si}$ , in the relaxed structures with 48 atoms. IR active local vibrational modes associated to the defects were observed for  $O_i$  and  $Si_i$  in a range of energies corresponding to the gap in the VDOS ( $729$  and  $743\text{ cm}^{-1}$  respectively). The eigenmodes are shown in Fig. 7. They mainly involve the stretching of Si-O bonds close to the interstitials. Other localized modes were observed for these point defects, but they are not IR active.

The crystal modes are affected by the presence of the defect. The changes are more important in  $Si_i$ , probably due to a stronger interaction with oxygen atoms around this interstitial. For  $O_i$ , the frequencies of the crystalline modes are almost unaffected (though some splittings are observed for the low frequency modes) showing that the defective structure does not differ much from the crystalline one. In the charged configuration ( $O_i^{-2}$ ), the interstitial is bonded to two silicon atoms, hence considerably affecting the vibrational modes of the Si-O tetrahedra. Some weak IR active modes appear in the gap for this defect. Zirconium interstitial affects mainly the low energy part of the spectra (below  $500\text{ cm}^{-1}$ ), where the Zr-O interactions are more important. The Si-O stretching modes are softer, probably due the increase in the distance between silicon tetrahedra, consequence of the large expansion in the *ab*-plane. For the anti-site defect  $Zr_{Si}$ , the high energy modes, involving the stretching of the tetrahedra bonds, are weaker. The low energy modes, mainly related to relative displacements of the Zr and Si-tetrahedra sublattices, are less affected.

## V. DISCUSSION

Experimentally, the change in the lattice parameters can be directly monitored using x-ray diffraction. Point defects would be randomly distributed through the crystal lattice. If the number of accumulated  $\alpha$ -decays is not too large ( $\sim 2 \times 10^{18}\alpha/g$ ), and we assume that  $\sim 220$  atoms are displaced by each  $\alpha$  particle<sup>7</sup>, we can expect concentrations of  $2 \times 10^{21}$  defects/cm<sup>3</sup>. That is roughly one defect for each two unit cells, the kind of concentration considered in this work. Similar concentrations have been used to study the effect of doping on the lattice parameters of semiconductors<sup>26</sup>, but the changes observed are considerably smaller ( $\sim 0.19\%$ ). We performed simulations of Si interstitials in the crystalline silicon struc-

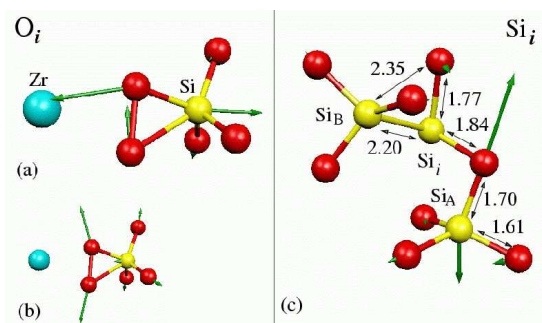


FIG. 7: (*Color online*) Local Vibrational Modes for  $O_i$  and  $Si_i$  point defects. (a) and (b) show the eigenmodes for oxygen interstitial at  $729\text{ cm}^{-1}$  (IR active) and  $870\text{ cm}^{-1}$  respectively. (c) shows the IR active mode for silicon interstitial at  $734\text{ cm}^{-1}$ . The relatively high frequency of mode (b) is an indication of the bond strength between the oxygens in the dumbbell. (Distances in Å)

ture with a supercell of 64 atoms (roughly the same concentration of defects), giving a volume swelling of 0.2%, much smaller than the values obtained for zircon with the same approach. In ceramic materials used for nuclear applications radiation swelling is more important ( $\Delta V/V$  up to 8% in SiC) and both defect accumulation and ratio between amorphized and crystalline phases play an important role<sup>27</sup>.

When compared with experiments, our calculations at those concentrations, single out three candidates as possible originators of the lattice swelling:  $O_i$ ,  $Si_i$  and  $Zr_{Si}$ . Some concentration of these three defects should be there to account for the experimental findings, even if other defects can be present at lower concentrations. In the following we discuss the compatibility of this conclusion with other facts known about the system.

For weakly damaged zircon, the fraction of crystalline phase is larger than the fraction of amorphized regions, and the diffraction maxima are weaker than in undamaged crystals. The anisotropic thermal displacement factors have been used to quantify the effect of the radiation damage in zircon<sup>7</sup>, indicating that the damage has more important effects on Zr and O atoms than on Si, which remain inside the  $SiO_4$  tetrahedral units due to the stronger binding of Si with O. In contrast with these findings, calculations of threshold displacement energies<sup>9</sup> ( $E_d$ ) show that for neutral atoms  $E_d(O) \ll E_d(Si) \approx E_d(Zr)$ .

However, it is important to emphasize that  $E_d$  can change substantially with the charge state. Charged defects can migrate through the lattice with a lower migration energy than neutral ones. In fact, the atomic configurations for oxygen interstitials are similar to the ones observed for  $ZrO_2$  and  $HfO_2$ <sup>24,29</sup>. In these materials, oxygen is incorporated and diffuses in atomic form, acting as an electron trap, while neutral defects tend to form strong bonds with other lattice oxygens. The negative-U behaviour favors the appearance of charged interstitials that are less tightly bound to other oxygens.

In a real material, we can expect all kind of defects being present, with the swelling produced by some of them being compensated with the deflation due to others. The presence of interstitials requires that vacancies are formed somewhere in the lattice, but the effect of these vacancies on the lattice parameters is smaller (see Fig. 2). The formation of  $Zr_{Si}$  leaves a  $V_{Zr}$  and a interstitial of Si. The combination of these three defects is compatible with a larger swelling along the  $c$ -axis than in the  $ab$ -plane, as observed experimentally. The forma-

tion energies for the point defects studied<sup>18</sup>, indicate that the most probable defects would be interstitials of oxygen and the anti-site  $Zr_{Si}$ . Depending on the chemical potentials of each species ( $\mu_O$ ,  $\mu_{Si}$  and  $\mu_{Zr}$ ) interstitials of Si and Zr might be present. The IR active mode at  $\sim 730 \text{ cm}^{-1}$  would give further evidence for the presence of oxygen, and maybe silicon, interstitials.

<sup>29</sup>Si nuclear magnetic resonance studies of damaged zircon indicate changes in the Si local environment towards a polymerization of the structure<sup>28</sup> during amorphization. This means that Si–O–Si bonds are formed in the amorphous region and the initially isolated  $SiO_4$  tetrahedra are connected through an oxygen bridge. This polymerization requires that on average the number of oxygens per Si is smaller in the amorphized region, favouring the presence of interstitial oxygens in the rest of the system. As we have seen  $O_i^{-2}$  forms bridging structures between Si atoms. But also the presence charged Si interstitials can give similar polymerization and change the chemical shifts of crystalline Si.

## VI. CONCLUSIONS

Simulations of high concentration of point defects in  $ZrSiO_4$  have been performed to study the effect of these on the lattice swelling under radiation damage. Using different sizes for the host crystalline supercell, we obtain various concentrations of periodically repeated defects. A roughly linear dependence between the swelling and the defect concentration has been observed for these ordered defective crystal. Based on experimental evidence of anisotropic swelling, we have selected a set of defects as good candidates to be responsible for the lattice expansion in crystalline zircon. Vibrational properties in radiation damaged samples are also used to justify our conclusions. These include interstitials of oxygen and silicon, and the anti-site defect  $Zr_{Si}$ .

## VII. ACKNOWLEDGMENTS

This work was supported by British Nuclear Fuels (BNFL) and NERC. We would like to thank E. K. H. Salje, M. T. Dove, K. Trachenko, M. Yang, S. Rios, I. Farnan for helpful discussions on radiation damage.

\* Corresponding Author: mpru02@esc.cam.ac.uk

† Present address: Physics Department, Trinity College, Dublin, Ireland.

<sup>1</sup> W. J. Weber *et al.*, *J. Mater. Res.* **13**, 1434 (1998).

<sup>2</sup> K. E. Sickafus, L. Minervini, R. W. Grimes, J. A. Valdez, M. Ishimaru, F. Li, and K. J. McClellan, *Science* **289**, 5479 (2000).

<sup>3</sup> G. D. Wilk and R. M. Wallace, *Appl. Phys. Lett.* **76**, 112 (2000).

<sup>4</sup> R. C. Ewing, W. Lutze, and W. J. Weber, *J. Mater. Res.* **10**, 243 (1995).

<sup>5</sup> H. D. Holland and D. Gottfried, *Acta Cryst.* **8**, 291 (1955).

<sup>6</sup> W. J. Weber, *J. Am. Ceram. Soc.* **76**, 1729 (1993).

<sup>7</sup> S. Ríos, T. Malcherek, E. K. H. Salje, and C.

- Domeneghetti, *Acta Cryst.* **B56**, 947 (2000).
- <sup>8</sup> J.-P. Crocombette, *Phys. Chem. Minerals* **27**, 138 (1999).
- <sup>9</sup> B. Park, W. J. Weber, L. R. Corrales, *Phys. Rev. B* **64**, 174108 (2001).
- <sup>10</sup> P. Ordejón, E. Artacho, and J. M. Soler, *Phys. Rev. B* **53**, 10441 (1996); J. M. Soler, E. Artacho, J. D. Gale, A. García, J. Junquera, P. Ordejón and D. Sánchez-Portal, *J. Phys.: Condens. Matter* **14**, 2745 (2002).
- <sup>11</sup> P. Hohenberg and W. Kohn, *Phys. Rev.* **136**, B864 (1964); W. Kohn and L. J. Sham, *Phys. Rev.* **140**, A1133 (1965).
- <sup>12</sup> D. M. Ceperley and B. J. Alder, *Phys. Rev. Lett.* **45**, 566 (1980).
- <sup>13</sup> N. Troullier and J. L. Martins, *Phys. Rev. B* **43**, 1993 (1991).
- <sup>14</sup> L. Kleinman and D.M. Bylander, *Phys. Rev. Lett.* **48**, 1425 (1982).
- <sup>15</sup> J. Junquera, O. Paz, D. Sánchez-Portal, and E. Artacho, *Phys. Rev. B*, **64**, 235111 (2001).
- <sup>16</sup> The basis was optimized to minimize the energy of  $\text{ZrO}_2$  with a fictitious pressure of 0.2 GPa with the method described in E. Anglada, J. M. Soler, J. Junquera, and E. Artacho, *Phys. Rev. B*, **66**, 205101 (2002).
- <sup>17</sup> G. Makov, and M. C. Payne, *Phys. Rev. B* **51**, 4014 (1995).
- <sup>18</sup> M. Pruneda and E. Artacho, (to be published).
- <sup>19</sup> M. Zhang and E. K. H. Salje, *J. Phys. Condens. Matter* **13**, 3057 (2001).
- <sup>20</sup> X. Gonze and C. Lee, *Phys. Rev. B* **55**, 10355 (1997).
- <sup>21</sup> R. D. King-Smith and D. Vanderbilt, *Phys. Rev. B* **47**, 1651 (1993).
- <sup>22</sup> G.-M. Rignanese, X. Gonze, A. Pasquarello, *Phys. Rev. B* **63**, 104305 (2001).
- <sup>23</sup> K. Robinson, G. V. Gibbs, P. H. Ribbe, *Am. Mineral.* **56**, 782 (1971).
- <sup>24</sup> A. S. Foster, V. B. Sulimov, F. Lopez Gejo, A. L. Shluger and R. M. Nieminen, *Phys. Rev. B* **64**, 224108 (2001).
- <sup>25</sup> M. Zhang, E. K. H. Salje, R. C. Ewing, I. Farnan, S. Ríos, J. Schlüter, P. Leggo, *J. Phys. Condens. Matter* **12**, 5189 (2000).
- <sup>26</sup> G. S. Cargill, III, J. Angilello, and K. L. Kavanagh, *Phys. Rev. Lett.* **61**, 1748 (1988).
- <sup>27</sup> F. Gao and W. J. Weber, *Nucl. Instrum. and Meth. B* **207**, 10 (2003).
- <sup>28</sup> I. Farnan and E. K. H. Salje, *J. Appl. Phys.* **89**, 2084 (2001).
- <sup>29</sup> A. S. Foster, F. Lopez Gejo, A. L. Shluger, and R. M. Nieminen, *Phys. Rev. B* **65**, 174117 (2002).